Int. J. Solids Structures Vol. 30, No. 6, pp. 779–795, 1993
Printed in Great Britain

0020–7683/93 $6.00+ .00

EFFECTS OF RESIDUAL STRESSES IN THE BLISTER TEST

H. M. JENSEN
Department of Solid Mechanics, The Technical University of Denmark, DK-2800 Lyngby, Denmark

and

M. D. THOULESS
IBM Research Division, T. J. Watson Research Center, Yorktown Heights, NY 10598, U.S.A.

(*Received* 4 *March* 1992; *in revised form* 18 *September* 1992)

Abstract—An analysis of the blister test, which is used as a method for measuring the fracture toughness of interfaces, is presented. The fracture toughness has been determined as a function of the critical loads needed to cause delamination. In most thin-film composites, residual stresses are present and the effect of these is incorporated in the analysis. For isotropic materials with equi-biaxial residual stresses, and a pressure or a point load applied to the film, the fundamental shape of the delamination is circular due to symmetry. Closed-form solutions for the energy-release rate and mixedness of modes have been derived for circular crack fronts. One effect of compressive in-plane stresses is a possible loss of stability of the circular crack front. Numerical results for the combinations of normal loads and residual stresses which result in crack front instabilities have been obtained and compared with experimental observations.

1. INTRODUCTION

The blister test (Fig. 1) is often used as a method for measuring the toughness of an interface. In this test, a thin film attached to a substrate is delaminated by means of either a point load or an internal pressure, and a value for the interfacial toughness is determined from the geometry of the blister and the magnitude of the applied loads. Approximate analyses of this test were originally given by Bennett *et al.* (1974) and Malyshev and Salganik (1965); recently, a more rigorous solution has been given by Jensen (1991). These analyses do not include the residual stresses often present in thin-film composites which may be induced by the deposition process, thermal-expansion mismatch between the film and substrate, or by bending of the composite. The analysis presented in this paper does incorporate the effects of these stresses, and it will be seen that they can have a profound influence on the behaviour of the blister test.

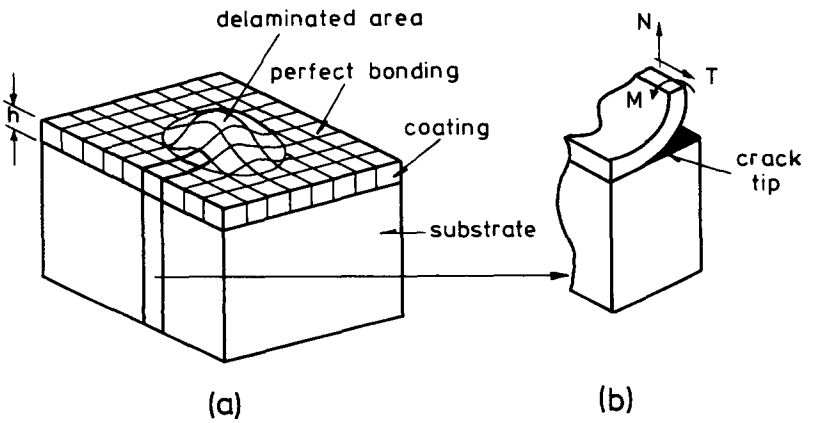

Fig. 1. (a) A thin coating which has delaminated from the substrate. A section at the boundary between the bonded and delaminated zone is shown in (b), where the effective stresses and moments loading the crack are also shown.

The analysis is performed by coupling the basic results for an interface crack with the membrane stresses and bending moments obtained by treating the film as a thin plate clamped to a substrate. Owing to the type of loadings considered, and to the assumed isotropy of the materials, the initial shape of the delaminated area is circular. Closed-form and numerical solutions for the energy-release rate and its separation into mode-1 and mode-2 components are obtained for this shape. However, a stability analysis reveals that, if there is a residual compressive stress, this shape can lose its stability as delamination proceeds. As discussed in Hutchinson *et al.* (1992), there are two types of instability: a buckling instability for the detached film, and a configurational instability for the crack front. Both of these types are also identified in the present work.

The paper is organized so that, first, the basic results for an interface crack are reviewed. The general results obtained by Suo and Hutchinson (1990) for the separation of the energy-release rate into mode-1 and mode-2 components are particularly important for the rest of the analysis, as is the necessity of formulating a failure criterion which incorporates the strong dependence of interface toughness on the relative amounts of mode 1 and mode 2. The governing plate equations are then used to analyse the film deformation, and the results are coupled with the basic crack solutions. This allows closed-form solutions for the energy-release rate to be obtained for small deformations, and numerical solutions to be obtained for arbitrary deformations. A perturbation analysis is performed in Section 2.3, and criteria for the instability of the crack front and for bifurcation buckling of the film are formulated. Finally, Section 3 contains a description of some model experiments which investigated the effects of residual stresses in a blister test; the results of these experiments are compared with the theoretical predictions.

2. ANALYSIS

The system considered in the following analysis is is sketched in Fig. 1. A thin film is bonded to a substrate with an initial region of delamination that has been formed by external loading, residual stresses, contamination or other causes; further delamination is assumed to occur as a result of a constant pressure, a point load applied normal to the surface of the film or residual, equi-biaxial, in-plane stresses. It is assumed that there is a distinct boundary between the bonded and the delaminated area which can be treated as an interface-crack tip. Both materials are assumed to be linear-elastic and isotropic, but the elastic moduli for the film and substrate, E and E_s, may be different, as may the Poisson's ratios, ν and ν_s. The film thickness, h, is assumed to be small compared to the thickness of the substrate, the extent of the delamination and the radius of curvature of the crack front. This ensures that plane-strain conditions hold locally along the crack front, and allows the analysis to be split in two separate parts: the membrane stresses and bending moments along the boundary are found by treating the film as a thin plate clamped to the substrate, these are then identified with the loads acting on the interface crack to deduce the fracture mechanics of the delamination.

2.1. *Edge crack at an interface*

First, the basic, bimaterial interface-crack solutions that are needed in the analysis are reviewed. For the plane-strain interface-crack shown in Fig. 2, the energy-release rate, G, is

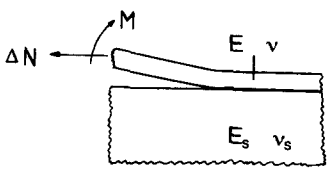

Fig. 2. Plane-strain interface crack problem with sign conventions for the effective membrane force and the bending moment.

$$G = \frac{6(1-\nu^2)}{Eh^3}\left[M^2 + \frac{h^2}{12}\Delta N^2\right], \tag{1}$$

where ΔN denotes the change from the original state of the in-plane stress. The mode-1 and mode-2 stress-intensity factors, K_1 and K_2, are defined such that the tractions a distance x ahead of the crack tip are $\sigma_{22}+i\sigma_{12} = (K_1+iK_2)x^{i\varepsilon}/\sqrt{2\pi x}$ where $i = \sqrt{-1}$. In terms of M and ΔN, K_1 and K_2 are given by

$$K_1+iK_2 = -\left[\frac{\Delta N}{\sqrt{2h}} + iM\sqrt{\frac{6}{h^3}}\right]\sqrt{\frac{1-\alpha}{1-\beta^2}}\, h^{-i\varepsilon} e^{i\omega}, \tag{2}$$

where $\omega(\alpha, \beta)$ is a function tabulated in Suo and Hutchinson (1990). A measure of mode mixedness, the phase angle ψ, is defined by

$$\tan\psi \equiv \frac{\mathrm{Im}\,[h^{i\varepsilon}(K_1+iK_2)]}{\mathrm{Re}\,[h^{i\varepsilon}(K_1+iK_2)]} = \frac{\sqrt{12}M\cos\omega + h\Delta N\sin\omega}{-\sqrt{12}M\sin\omega + h\Delta N\cos\omega}. \tag{3}$$

With $\tilde{E} = E/(1-\nu^2)$, the Dundurs' parameters, α and β, and the bimaterial constant, ε, are

$$\left.\begin{aligned} \alpha(\tilde{E}+\tilde{E}_s) &= \tilde{E}-\tilde{E}_s \\ 2\beta(\tilde{E}+\tilde{E}_s) &= \tilde{E}(1-2\nu_s)/(1-\nu_s) - \tilde{E}_s(1-2\nu)/(1-\nu) \\ \varepsilon &= \frac{1}{2\pi}\ln\frac{1-\beta}{1+\beta} \end{aligned}\right\}. \tag{4}$$

Next, a fracture criterion must be defined for the interface crack loaded under mixed-mode conditions. As in Jensen *et al.* (1990), this is defined using the general expression for the energy-release rate of an interface crack. In the absence of mode 3, failure is assumed to occur when K_1 and K_2 reach values such that the expression

$$\frac{1}{2\cosh^2\pi\varepsilon}\left(\frac{1}{\tilde{E}}+\frac{1}{\tilde{E}_s}\right)(K_1^2+\lambda K_2^2) = G_{1c} \tag{5a}$$

is satisfied, where G_{1c} is the mode 1 toughness and λ ($0 \leqslant \lambda \leqslant 1$) is chosen to fit experimental results for a given bimaterial interface. For $\lambda = 1$, (5a) is the Griffith fracture criterion for perfectly brittle materials. For $\lambda < 1$, (5a) is regarded as a phenomenological interface fracture criterion. It compares with the micromechanical model of Evans and Hutchinson (1989) for $\alpha = \beta = 0$, in that $\lambda = 0$ and $\lambda = 1$ correspond to rough and smooth interfaces, respectively. In Jensen *et al.* (1990), $\lambda = 0.15$ gave good agreement with experimental results for a polyimide/glass system. For $\beta = 0$, the criterion (5a) is identical to

$$\left.\begin{aligned} G &= G_{1c}\cdot f(\psi) \\ f(\psi) &= (1+(\lambda-1)\sin^2\psi)^{-1} \end{aligned}\right\}, \tag{5b}$$

with ψ given by (3). In Hutchinson and Suo (1992), alternative functional expressions for $f(\psi)$ have been proposed. Incidentally, it should be noted that the analysis is not restricted to interfaces with $\beta = 0$, but the effect of contacting crack sides is neglected.

2.2. *Axisymmetric analysis*

The delaminated coating is treated as a thin plate, so that the equations describing the deformation of the blister can be formulated in terms of the normal displacement w and a stress function Φ. These equations, known as the von Karman equations (Niordson, 1985) have the general form

$$D\Delta^2 w = L[w, \Phi] + p, \tag{6}$$

$$\Delta^2 \Phi = -\frac{Eh}{2} L[w, w], \tag{7}$$

where Δ^2 is the biharmonic operator, D is the bending stiffness, p is the normal load, and the bilinear operator L is defined through the alternating tensor $\varepsilon_{\alpha\beta}$

$$L[w, \Phi] = \varepsilon^{\alpha\xi}\varepsilon^{\beta\eta} w_{,\xi\eta} \Phi_{,\alpha\beta}, \tag{8}$$

with $(\ )_{,\alpha}$ denoting covariant differentiation.

Equations (6), describing moment equilibrium of the plate, and (7), describing compatibility, can be simplified for axisymmetric deformation of a circular plate

$$Dr\left(\frac{1}{r}(r\theta)'\right)' - \phi\theta = \int_0^r p(\xi)\xi \, \mathrm{d}\xi, \tag{9}$$

$$r\left(\frac{1}{r}(r\phi)'\right)' + \frac{Eh}{2}\theta^2 = 0, \tag{10}$$

where $(\ )' = \mathrm{d}(\ )/\mathrm{d}r$, $\theta = w'$, $\phi = \Phi'$ and r is the distance to the plate centre. The effect of initial prestress is modelled by measuring the in-plane stresses and displacements from the initial state. This is done by substituting ϕ by $\phi - \sigma hr$ in (9) and (10) where σ is the prestress ($\sigma > 0$ in compression). In non-dimensional form, (9) and (10) become

$$\rho \frac{\mathrm{d}}{\mathrm{d}\rho}\left[\frac{1}{\rho}\frac{\mathrm{d}(\rho\bar{\theta})}{\mathrm{d}\rho}\right] - \bar{\phi}\bar{\theta}12(1-\nu^2) = q - \frac{\sigma}{\sigma_c} 14.68 \cdot \bar{\theta}\rho, \tag{11}$$

$$\rho \frac{\mathrm{d}}{\mathrm{d}\rho}\left[\frac{1}{\rho}\frac{\mathrm{d}(\rho\bar{\phi})}{\mathrm{d}\rho}\right] + \tfrac{1}{2}\bar{\theta}^2 = 0, \tag{12}$$

$$\rho = r/R, \quad \bar{\theta} = R\theta/h, \quad \bar{\phi} = R\phi/Eh^3. \tag{13}$$

Here, σ_c is the in-plane buckling stress of a clamped circular plate

$$\sigma_c = 14.68D/(hR^2), \tag{14}$$

and R is the radius of the delaminated zone. The term q in (11) is dependent on whether the normal load is applied as a *constant pressure* $p(r) = p$ or as a *central point load* $p(r) = P\delta(r)/2\pi r$:

$$q = 6\frac{pR^4}{Eh^4}(1-\nu^2)\rho^2 = q_1\rho^2 \quad \text{for} \quad p(r) = p, \tag{15}$$

$$q = 6\frac{PR^2}{\pi Eh^4}(1-\nu^2) = q_2 \quad \text{for} \quad p(r) = P\delta(r)/2\pi r, \tag{16}$$

where $\delta(r)$ denotes the Dirac delta function.

The boundary conditions at the centre and at the clamped edge are

$$\left.\begin{aligned} &\bar{\theta}(0) = 0, \quad \bar{\phi}(0) = 0 \\ &\bar{\theta}(1) = 0, \quad \frac{\mathrm{d}\bar{\phi}(1)}{\mathrm{d}\rho} = \nu\bar{\phi}(1) \end{aligned}\right\}. \tag{17}$$

Inspection of these boundary conditions and the governing equations (11) and (12) shows that the problem has three independent parameters q, σ/σ_c and ν.

In eqns (11) and (12), non-linear terms allowing for large deflections of the plate ($w > h$) are retained. But the surface rotations and strains have to be small. The exact solution to (11) and (12) in the linear, small displacement limit is

$$\left.\begin{aligned} &\bar{\phi} = 0 \\ &\bar{\theta}_h = aJ_1(k\rho) + bN_1(k\rho) \quad \text{for} \quad \sigma > 0 \\ &\bar{\theta}_h = aI_1(k\rho) + bK_1(k\rho) \quad \text{for} \quad \sigma < 0 \\ &k = \sqrt{14.68|\sigma|/\sigma_c} \end{aligned}\right\}, \tag{18}$$

where J_1, N_1, I_1 and K_1 are Bessel functions and modified Bessel functions of the first and second kind, and of order one. In (18), $\bar{\theta}_h$ denotes the solution to the homogeneous part of (11). The full solution is $\bar{\theta} = \bar{\theta}_h + \bar{\theta}_i$ where $\bar{\theta}_i$ is a particular solution to (11) which is dependent on whether the normal load is applied as a pressure (15) or as a point load (16):

$$\left.\begin{aligned} &\bar{\theta}_i = \frac{q_1\sigma_c}{14.68\sigma}\rho, \quad p(r) = p \\ &\bar{\theta}_i = \frac{q_2\sigma_c}{14.68\sigma}\frac{1}{\rho}, \quad p(r) = P\delta(r)/2\pi r \end{aligned}\right\}. \tag{19}$$

The constants a and b in (18) are determined from the boundary conditions (17). The bending moment M and membrane stress change ΔN, from which G and ψ are calculated, follow from the constitutive equation

$$M = D\theta' \tag{20a}$$

and the definition of the stress function

$$\Delta N = \phi'. \tag{20b}$$

By combining (18)–(20) and (1), the following results for G and ψ are obtained for *constant pressure*:

$$\left.\begin{aligned} G &= G_0 16\left(\frac{2}{k^2} - \frac{J_0(k)}{kJ_1(k)}\right)^2, \quad \sigma > 0 \\ G &= G_0 16\left(\frac{2}{k^2} - \frac{I_0(k)}{kI_1(k)}\right)^2, \quad \sigma < 0 \end{aligned}\right\} \psi = \omega - \frac{\pi}{2}, \tag{21}$$

where G_0 is the energy-release rate in the absence of a prestress:

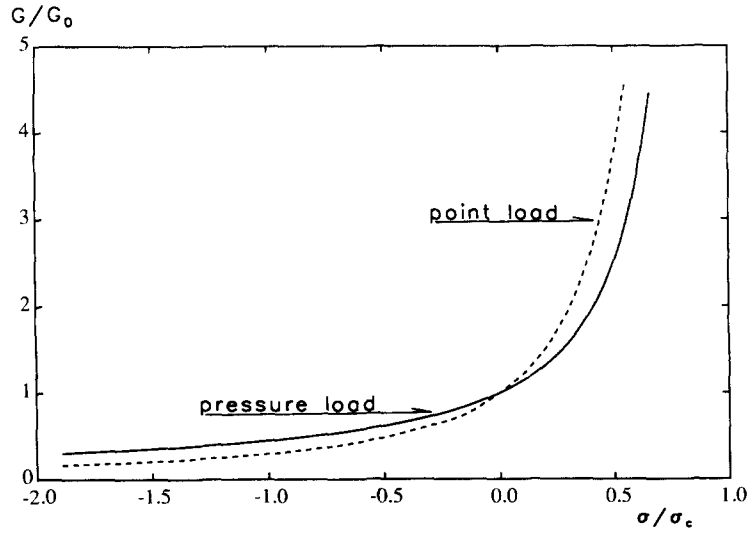

Fig. 3. Energy-release rate as a functional of residual stress for both the point-loaded and the pressurized coating for small deflections, as given by (21) and (23). The equi-biaxial residual stress σ is positive for compression and negative for tension.

$$G_0 = \frac{3(1-\nu^2)R^4p^2}{32Eh^3}. \tag{22}$$

The variation of G/G_0 with σ/σ_c is shown in Fig. 3. The energy-release rate, G, takes the following form for a *central point load*:

$$\left.\begin{aligned} G &= G_0 4\left[\left(1+\frac{\pi}{2}kN_1(k)\right)\frac{1}{kJ_1(k)}\frac{dJ_1(k)}{dk} - \frac{\pi}{2}\frac{dN_1(k)}{dk} + \frac{1}{k^2}\right]^2, \quad \sigma > 0 \\ G &= G_0 4\left[(1-kK_1(k))\frac{1}{kI_1(k)}\frac{dI_1(k)}{dk} + \frac{dK_1(k)}{dk} + \frac{1}{k^2}\right]^2, \quad \sigma < 0 \end{aligned}\right\}, \tag{23}$$

where, now, the energy-release rate in the absence of residual stresses, G_0, is given by

$$G_0 = \frac{3(1-\nu^2)P^2}{8\pi^2Eh^3}. \tag{24}$$

This variation of G/G_0 with σ/σ_c is included in Fig. 3. The phase angle ψ is the same as for the pressurized case (21). These solutions are valid for small deflections only, but they illustrate the influence of residual stresses. Note, that during the debond process, σ/σ_c is not constant due to the $1/R^2$ dependence of σ_c (14).

For large deflections, eqns (11) and (12) are solved numerically using a standard finite-difference method. It is, however, possible to solve (11) and (12) exactly in the limits of high pressure (Jensen, 1991). In the following sections, the main focus is on configurational instability, but some results illustrating the influence of residual stresses on G and ψ in the non-linear regime are shown in Figs 4–8. In Figs 4 and 5, the variations with pressure are shown regarding the residual stress σ/σ_c as a parameter. In Figs 6 and 7 the variations in G and ψ are shown as functions of σ/σ_c regarding the point load as a parameter. Finally, Fig. 8 shows the central deflection of the blister as a function of point load and residual stress. The figure is used in Section 3 to deduce P from measurements of $w(0)$ and σ. The numerical results for G and ψ in the limit of small deflections agree with the analytical results (21) and (23) within 0.1%. These numerical solutions form the basis for the stability analysis in the following section.

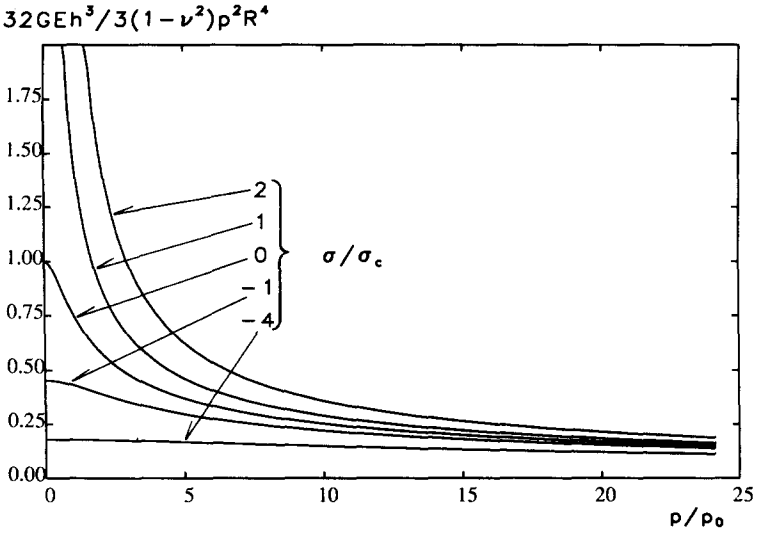

Fig. 4. Energy-release rate for large deflections as a function of non-dimensional constant pressure, p/p_0, where $p_0 = 16Eh^4/3(1-\nu^2)R^4$ and $\nu = 1/3$. The equi-biaxial, residual stress, σ, is positive for compression and negative for tension.

2.3. *Perturbation analysis*

In this section, a small perturbation to the axisymmetric solution of the previous section is introduced. The perturbation may be due to bifurcation buckling of the coating or it may be due to non-circular growth of the delamination. Distinction is made between these two sources as non-axisymmetric deformation of the coating limits the application of the solutions in Section 2.2.

A bifurcation and a perturbation of the circular crack front of the type

$$R_p = R(1+\varepsilon^* \cos(n\Omega)) \tag{25}$$

both result in perturbations of the independent variables given by

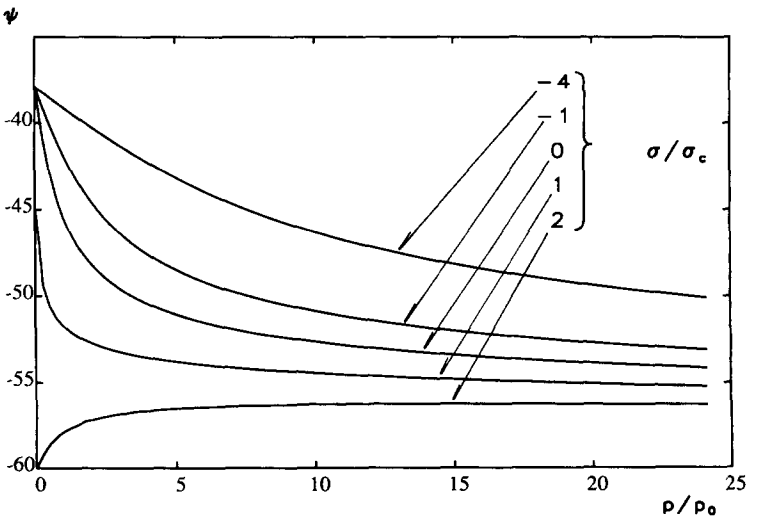

Fig. 5. Phase angle ψ for large deflections as a function of non-dimensional constant pressure, p/p_0, where $p_0 = 16Eh^4/3(1-\nu^2)R^4$, $\nu = 1/3$ and $\alpha = \beta = 0$. The equi-biaxial, residual stress, σ, is positive for compression and negative for tension. The exact asymptote for $p/p_0 \to \infty$ derived in Jensen (1991) is $\psi = -58.3°$.

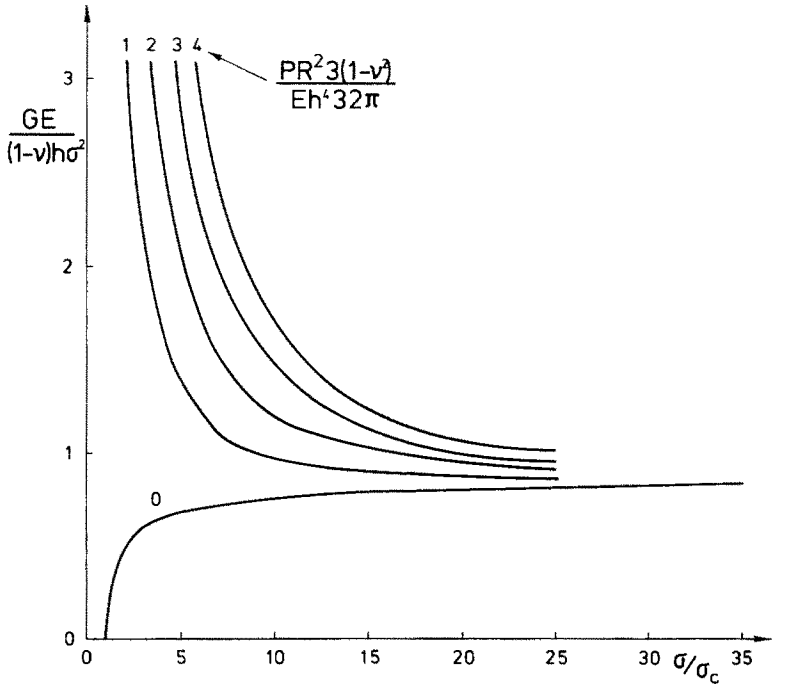

Fig. 6. Energy-release rate for large deflections as a function of residual stress for different values of point loads, P, on the coating, $\nu = 1/3$.

$$\begin{Bmatrix} w \\ \Phi \end{Bmatrix} = \begin{Bmatrix} w_0(r) \\ \Phi_0(r) \end{Bmatrix} + \varepsilon^* \cos(n\Omega) \begin{Bmatrix} w_n(r) \\ \Phi_n(r) \end{Bmatrix}, \tag{26}$$

where w_0 and Φ_0 are the axisymmetric solutions of Section 2.2, ε^* is the amplitude of the perturbation, n is the mode number and Ω is the circumferential angle. When (26) is inserted in (6) and (7), the governing equations for w_n and Φ_n become

$$D\Delta_n^2 w_n = \frac{1}{r}\left[(\theta\Phi_n' + \phi w_n')' - \frac{n^2}{r}(w_n\phi' + \theta'\Phi_n)\right], \tag{27}$$

$$\frac{1}{Eh}\Delta_n^2\Phi_n = -\frac{1}{r}\left[(\theta w_n')' - \frac{n^2}{r}\theta' w_n\right], \tag{28}$$

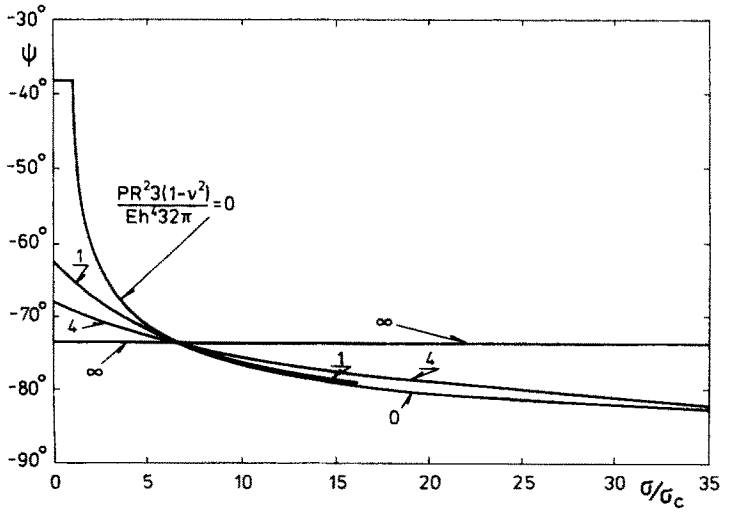

Fig. 7. Phase angle, ψ, for large deflections as a function of residual stress for different values of point loads, P, on the coating, $\nu = 1/3$ and $\alpha = \beta = 0$. The exact asymptote for $P \to \infty$ derived in Jensen (1991) ($\psi = -73.2°$) is included.

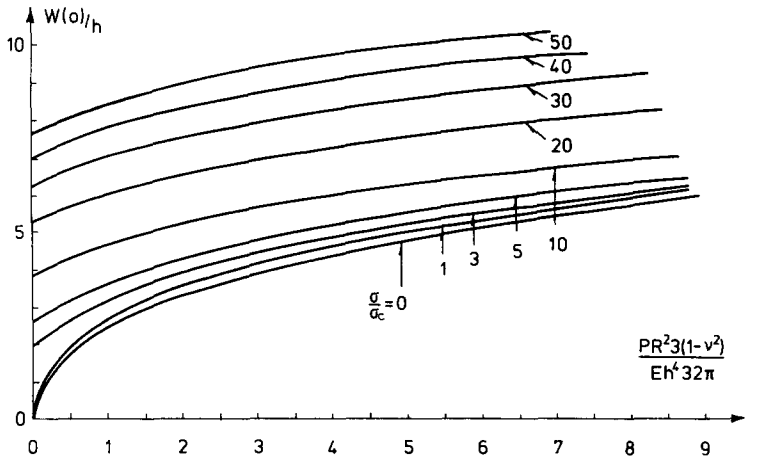

Fig. 8. Central deflection, $w(0)$, as a function of point load, P, at different levels of residual stress, σ, with $\nu = 1/3$.

where $\Delta_n(\ ) = (\ )''+(\ )'/r-n^2(\ )/r^2$. Equations (27) and (28) hold for both a bifurcation and a boundary perturbation. The boundary conditions, however, are different in the two cases. For a bifurcation, the coating is clamped to the substrate at $r = R$ giving

$$w_n(R) = 0, \quad w_n'(R) = 0, \tag{29}$$

$$u_n(R) = 0, \quad v_n(R) = 0, \tag{30}$$

where u_n and v_n are the in-plane radial and circumferential displacement *changes* from the prestressed state. In terms of Φ_n, (30) may be formulated as

$$\Phi_n''-\frac{\nu}{r}\Phi_n'+\frac{\nu n^2}{r^2}\Phi_n = 0, \tag{31}$$

$$r\Phi_n'''+\Phi_n''-\Phi_n'\frac{1}{r}(2n^2(1+\nu)+1-\nu n^2)+\Phi_n\frac{n^2}{r^2}(3+\nu) = 0. \tag{32}$$

In the case of a boundary perturbation, the coating is clamped but now at $r = R_p$ (25). If (25) is inserted in (26) and the displacements near $r = R$ are expanded in a Taylor series, then after collecting powers of ε*

$$w_n(R) = 0, \quad w_n'(R) = -R\theta'(R), \tag{33}$$

$$u_n(R) = -Ru_0'(R), \quad v_n(R) = 0, \tag{34}$$

where u_0 is the radial displacement change for the axisymmetric solution. Again, (34) may be formulated in terms of Φ_n by substituting the right-hand side in (31) with $-EhRu_0' = R(\nu^2-1)\phi(R)$ and in (32) with $-n^2EhRu_0'$. The perturbation problem was also formulated using in-plane displacements as independent variables. The boundary conditions (30) and (34) are simpler but the governing equations are more lengthy. The results for the two formulations agree within 0.3%.

The condition for bifurcation is that a non-trivial solution to the homogeneous problem (27), (28), (29) and (30) exists. The condition for stability of the boundary perturbation is strongy dependent on the interface fracture criterion (5). At first, the stress-intensity factors for the perturbation problem $K_{1,n}$ and $K_{2,n}$ are calculated using (2), the constitutive equation

$$M_n = D(w_n'' + \nu w_n'/r)\varepsilon^* \cos n\Omega, \tag{35}$$

and the definition of the stress function

$$\Delta N_n = (\Phi_n'/r - n^2\Phi_n/r^2)\varepsilon^* \cos n\Omega. \tag{36}$$

Now the total stress-intensity factors along the perturbated boundary are $K_{1,0}+\varepsilon^* \cos n\Omega K_{1,n}$ and $K_{2,0}+\varepsilon^* \cos n\Omega K_{2,n}$, where $K_{1,0}$ and $K_{2,0}$ are the stress-intensity factors for the circular boundary. When these are inserted into (5a), the fracture criterion becomes

$$\frac{1}{2\cosh^2 \pi\varepsilon}\left(\frac{1}{\bar{E}} + \frac{1}{\bar{E}_s}\right)(K_{1,0}^2 + \lambda K_{2,0}^2 + 2\varepsilon^* \cos n\Omega(K_{1,0}K_{1,n} + \lambda K_{2,0}K_{2,n})) = G_{1c}. \tag{37}$$

Here, terms of order $(\varepsilon^*)^2$ are neglected which include a mode 3 contribution from T (Fig. 1) where $T = n(\Phi_n'/r - \Phi_n/r^2)\varepsilon^* \sin n\Omega$. The general criterion for instability of a given crack shape to a perturbation is, as in Rice (1989) and Hutchinson *et al.* (1992), that the fracture criterion is exceeded on the parts of the crack front with the highest growth rate. Along the perturbed boundary (25), the growth rate is highest at the points where $\varepsilon^* \cos n\Omega > 0$. When this criterion is satisifed, the growth of the perturbation will be unbounded. Comparing (37) and (5a) and using this stability criterion the condition

$$G_n \equiv K_{1,0}K_{1,n} + \lambda K_{2,0}K_{2,n} \begin{cases} <0, & \text{circular crack stable,} \\ >0, & \text{circular crack unstable,} \end{cases} \tag{38}$$

is obtained. It is noted that the stability criterion could also be formulated on the basis of (5b).

The results of the bifurcation and perturbation analysis for a point loaded coating with compressive in-plane stresses are summarized in Fig. 9. The figure shows a map of the perturbation modes (25) which have the highest value of G_n (38) and thus are most likely to be observed. Below the lobes, the axisymmetric mode of delamination growth is stable. In the limit $P = 0$, delamination is purely buckle-driven, and the results are in good agreement with those of Hutchinson *et al.* (1992). Bifurcation occurs at $n = 8$ for small P, and at $n = 7$ or $n = 6$ for higher values of P. Above the bifurcation line, the small-perturbation analysis does not hold.

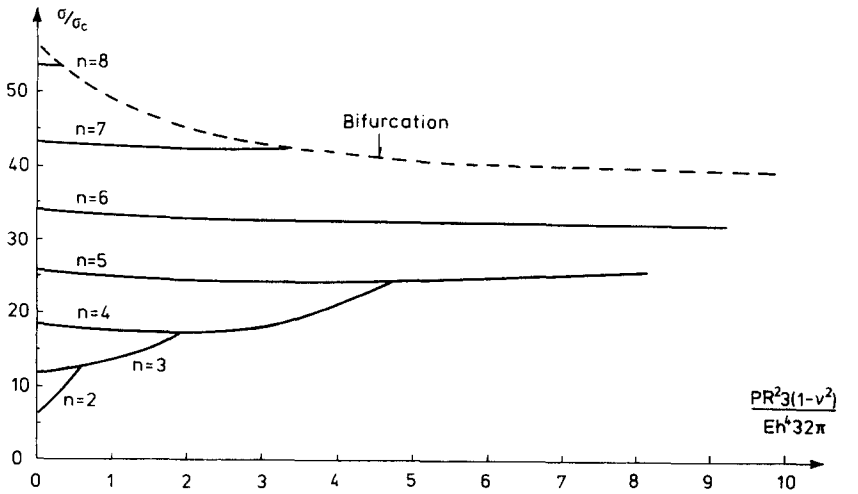

Fig. 9. Map of stable modes for perturbations of the circular crack front for combinations of point load, and compressive in-plane stresses, $\nu = 1/3$, $\alpha = \beta = 0$ and $\lambda = 0$.

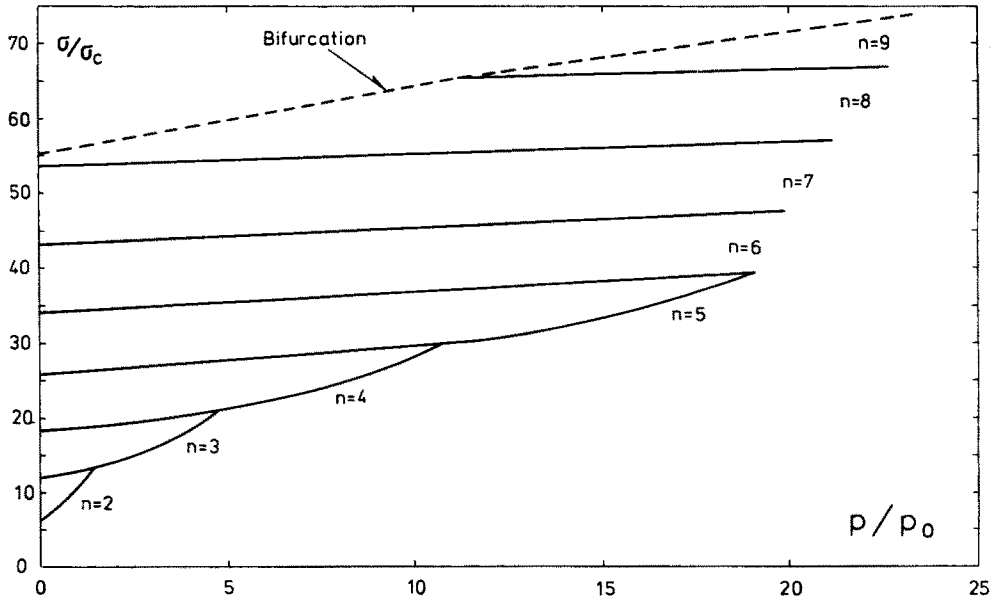

Fig. 10. Map of stable modes for perturbations of the circular crack front for combinations of pressure and compressive in-plane stresses, $p_0 = 16Eh^4/3(1-\nu^2)R^4$, $\nu = 1/3$, $\alpha = \beta = 0$ and $\lambda = 0$.

For completeness, a map of stable perturbation modes for a pressure-loaded coating in the presence of compressive in-plane stresses is shown in Fig. 10. From this map, and from that in Fig. 9, it is possible to see the regions where the solutions based on circular crack growth are valid. In particular, the blister test always results in circular delamination for systems with no, or tensile, residual stresses.

3. EXPERIMENTS

The theory developed in the previous section was compared to experimental observations made on a model system consisting of a film of mica bonded to an aluminum substrate by a thermoplastic resin† (Fig. 11) (Hutchinson *et al.*, 1992; Thouless *et al.*, 1992). The mica–resin interface was delaminated by means of a screw threaded through the back of the substrate and pushing against the back surface of the mica. The film-substrate assembly was placed on a heating/cooling stage and clamped to a rigid rig. As the blister developed, the displacement of the top surface of the mica was measured by a displacement gauge. Simultaneously, the shape and size of the delamination were observed by optical means. The residual stress in the mica, σ, was varied by heating or cooling the system and utilizing the differences in thermal expansion between the mica and aluminum. The temperature below which the resin behaved in an elastic fashion had been previously determined (Hutchinson *et al.*, 1992), so that, by measuring the temperature of the system,

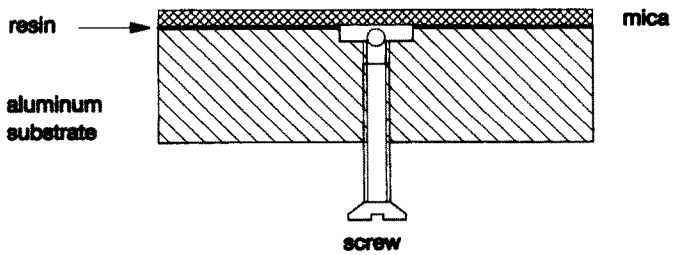

Fig. 11. The film-substrate assembly used to study the delamination behaviour of the blister test.

† Buehler Lakeside-80 Thermoplastic Cement.

and knowing the coefficients of thermal expansion of mica and aluminum, the magnitude of the residual stress could be calculated. The magnitude of the buckling stress, σ_c, for the portion of the film above the delamination was deduced from the diameter of the delamination. The ratio σ/σ_c could therefore be monitored throughout the experiments. This value, coupled with the displacement measurements, were then used to deduce the magnitude of the point load, the energy-release rate and the phase angle (Figs 6–8).

Figure 12 is a sequence of photographs of a blister showing how unstable perturbations to the crack front can affect an initially axisymmetric blister. This sequence was taken during one experiment conducted at a constant temperature with the delamination size being increased by means of the screw. Observations of the blister shape, coupled with measurements of σ/σ_c and P, allowed a map of the experimental data to be plotted (Fig. 13). This map is in good qualitative agreement with the theoretical predictions of Fig. 9; in particular the apparent suppression of the $n = 2$ nodes should be noted. As the blister developed, the energy-release rate and the phase angle for each configuration was calculated assuming that the blister maintained an approximately circular shape. The calculated value of G was then taken to be the fracture resistance of the mica–resin interface at the appropriate phase angle. The results are in agreement with data obtained for the same system but using a different geometry (Thouless *et al.*, 1992) and are plotted in Fig. 14. The error bars in this figure represent the uncertainty in the measurements; the largest contribution to these uncertainties came from the loss of axisymmetry.

4. DISCUSSION

A comparison of Figs 9 and 13 shows at least qualitative agreement between them; in particular, the lower modes of instability are suppressed by the imposition of a point load on a biaxially compressed coating. A number of factors may account for differences between the two figures. Probably the most important of these is that the analysis considered the development of small perturbations from an axisymmetric shape. In the experiments, perturbations often developed from a shape that was, in itself, an advanced perturbation of a circle. Other differences between the theory and experiments include the values assumed for the Dundurs' parameters and the assumed failure criterion. The results shown in Fig. 9 were obtained by Dundurs' parameters of $\alpha = \beta = 0$, and with $\lambda = 0$ in (5a). For the mica/aluminum system used in the experiments, $\alpha = 0.4$ and $\beta = 0.1$, and the data of Fig. 14 show that $\lambda = 0.15$ provides an approximate fit to (5a). The Dundurs' parameters affect the results only through $\omega(\alpha, \beta)$ appearing in (2) and (3). This is a small effect as can be seen from Suo and Hutchinson (1990), in which it is shown that $\omega(0,0) = 52.1^\circ$, while $\omega(0.4, 0.1) = 52.5^\circ$. The failure criterion has a more significant effect. As an example, Fig. 15 compares the results of the perturbation analysis of Section 2.3 for $\lambda = 0$ and $\lambda = 0.15$. With this higher value of λ, the lower instability modes are suppressed sooner while the modes with $n > 4$ are almost unaffected. At an extreme value of $\lambda = 1$, shape instabilities are predicted only when the values of σ/σ_c are close to the bifurcation limit, and only for modes with $5 \leqslant n \leqslant 8$. This sensitivity to λ emphasizes the importance of formulating appropriate mixed-mode failure criteria.

As is apparent from the non-dimensional equations (11) and (12), not only does the present analysis incorporate the effects of residual stresses on the blister test, but it is equally valid for investigating the effects of positive or negative normal loads on buckling-driven delamination. An example of such a situation might be when a vacuum develops between the film and substrate during delamination. In this particular example, the normal pressure is negative and acts only after the film has buckled away from the substrate. The present analysis applies to such a case without modification. But first, it should be noted that for buckle-driven delamination, a useful form of (5a) can be obtained by normalizing it with the elastic energy per unit area of the unbuckled film, $h(1-\nu)\sigma^2/E$. The failure criterion can then be expressed in the form

$$\sigma\sqrt{\frac{h(1-\nu)}{EG_{Ic}}} = g(\alpha, \beta, \lambda, \nu, \sigma/\sigma_c, p/p_0), \tag{39}$$

where, for short, g denotes the square root of the inverted and normalized left-hand side

Fig. 12. A sequence of photographs showing the development of the shape of the mica–resin interface. The delamination was propagated by means of a point load, and there was a residual stress in the film.

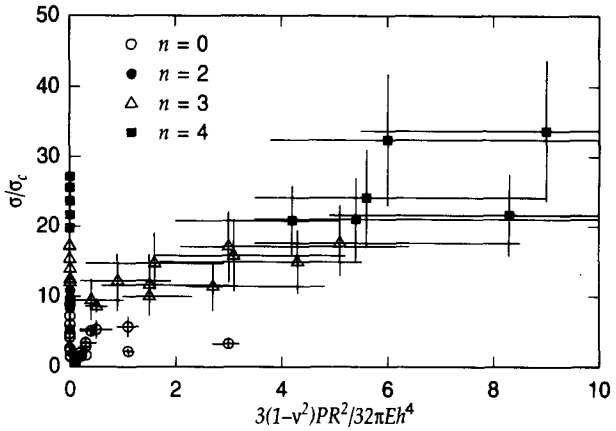

Fig. 13. A map illustrating the observed blister shape (n is the order of the crack-front perturbations) as a function of both σ/σ_c and the point load, P.

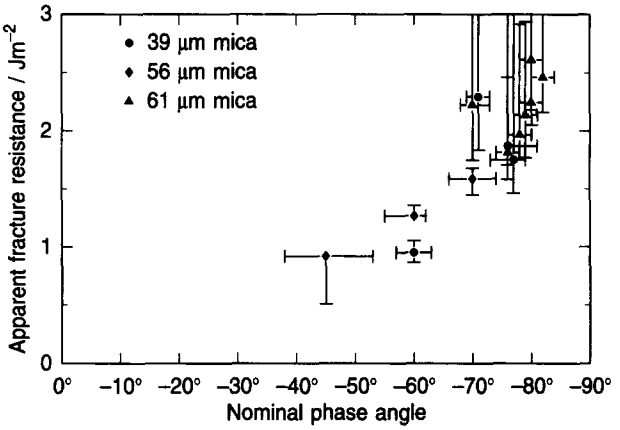

Fig. 14. Apparent fracture resistance of the mica–resin interface plotted as a function of the nominal phase angle.

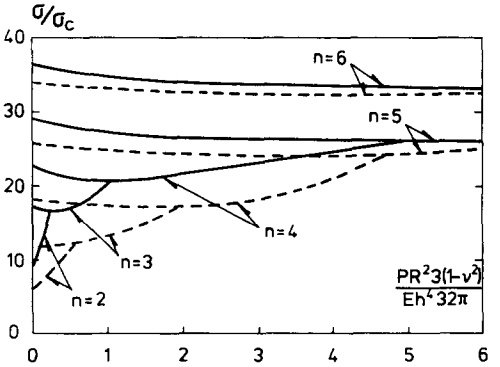

Fig. 15. Map of stable modes for perturbations of the circular crack front for combinations of point-load and compressive in-plane stresses, $\nu = 1/3$, $\alpha = \beta = 0$ and $\lambda = 0.15$. The dashed curves are the results for $\lambda = 0$ (Fig. 9).

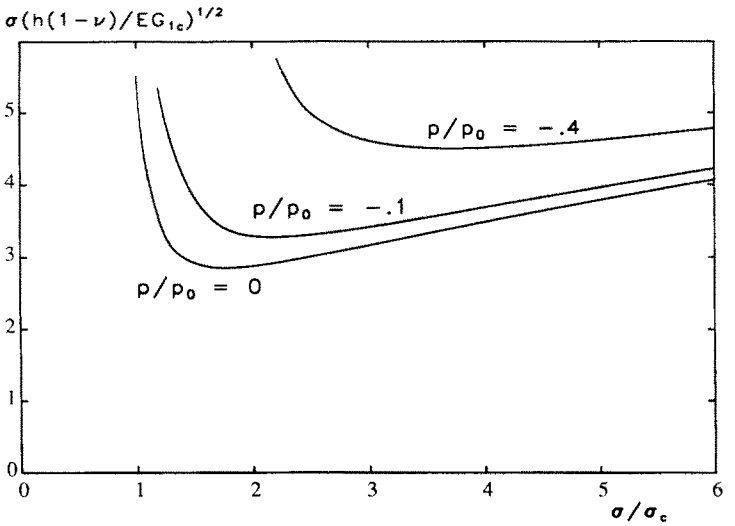

Fig. 16. Normalized and inverted fracture criterion (5a) for buckle-driven delamination including external pressure on the blister, $p_0 = 16Eh^4/3(1-\nu^2)R^4$, $\nu = 1/3$, $\alpha = \beta = 0$ and $\lambda = 0$.

of (5a). In Fig. 16, the variation of g evaluated from the numerical procedure of Section 2.2 is shown for $\alpha = \beta = 0$, $\lambda = 0$ and $\nu = 1/3$. The plot is particularly interesting as it clearly demonstrates the stabilizing effect of an internal vacuum.

5. CONCLUSION

The blister test for measuring adhesion of thin coatings has been analysed. Both the pressurized and the point-loaded cases were considered, as well as the effects of residual, in-plane stresses. The boundary between the bonded and the delaminated areas was treated as the tip of an interface crack. First, the deformation of the coating under the applied loads was found by considering the coating to be a thin plate clamped to the substrate at the boundary of the delaminated zone. The effective stresses and moments at the clamped boundary were then taken to be the loads acting on the interface-crack tip. Closed-form solutions for the energy-release rate and mode mixedness were obtained in the limit of small displacements of the coating. These solutions assumed that the fundamental shape of the delamination was circular, as would be the case for isotropic materials, axisymmetric normal loadings and equi-biaxial, in-plane stresses. For large deflections, the energy-release rate and mixedness of modes were found by a numerical procedure. The solutions presented are valid not only for blister tests, but equally well simulate the influence of normal loading on buckling delamination. The effects of normal loads should be considered for buckle-driven delamination when, for instance, a vacuum develops between the film and the substrate after delamination, creating an external pressure on the coating. The present results carry over without changes in these cases.

In addition to affecting the energy-release rate and phase angle, residual stresses in the coating can induce a loss of stability of the circular delamination shape. This effect was studied in detail, and experimental results showed good agreement with the theory.

Acknowledgements—The contributions of E. G. Liniger to the experimental measurements are gratefully acknowledged.

REFERENCES

Bennett, S. J., Devries, K. L. and Williams, M. L. (1974). Adhesive fracture mechanics. *Int. J. Fract.* **10**(1), 33–43.

Evans, A. G. and Hutchinson, J. W. (1989). Effects of non-planarity on the mixed mode fracture resistance of bimaterial interfaces. *Acta Metall. Mater.* **37**, 909–916.

Hutchinson, J. W. and Suo, Z. (1992). Mixed mode cracking in layered materials. *Adv. Appl. Mech.* **29**, 64–187.

Hutchinson, J. W., Thouless, M. D. and Liniger, E. G. (1992). Growth and configurational stability of circular, buckling-driven film delaminations. *Acta Metall. Mater.* **40**(2), 295–308.

Jensen, H. M. (1991). The blister test for interface toughness measurement. *Engng Fract. Mech.* **40**(3), 475–486.

Jensen, H. M., Hutchinson, J. W. and Kim, K.-S. (1990). Decohesion of a cut pre-stressed film on a substrate. *Int. J. Solids Structures* **26**(9/10), 1099–1114.

Malyshev, B. M. and Salganik, R. L. (1965). The strength of adhesive joints using the theory of cracks. *Int. J. Fract. Mech.* **5**, 114–128.

Niordson, F. I. (1985). *Shell Theory*. North-Holland, Amsterdam.

Rice, J. R. (1989). Weight function theory for three-dimensional elastic crack analysis. *ASTM-STP 1020 Proc., Fract. Mech.* 29–57.

Suo, Z. and Hutchinson, J. W. (1990). Interface crack between two elastic layers. *Int. J. Fract.* **43**, 1–18.

Thouless, M. D., Hutchinson, J. W. and Liniger, E. G. (1992). Plane-strain buckling-driven delamination of thin films: Model experiments and mode-II fracture. *Acta Metall. Mater.* **40**(10), 2639–2649.